Received: 16 March 2022 | Revised: 6 June 2022 | Accepted: 7 June 2022

DOI: 10.1111/mmi.14952

RESEARCH ARTICLE

WILEY

The transmembrane α-helix of LptC participates in LPS extraction by the $LptB_2FGC$ transporter

Andrew Wilson | **Natividad Ruiz**

Department of Microbiology, The Ohio State University, Columbus, Ohio, USA

Correspondence
Natividad Ruiz, Department of Microbiology, The Ohio State University, Columbus, OH, USA.
Email: ruiz.82@osu.edu

Funding information
National Institute of General Medical Sciences, Grant/Award Number: R01-GM100951 and T32-GM086252

Abstract

Lipopolysaccharide (LPS) is an essential component of the outer membrane of most Gram-negative bacteria that provides resistance to various toxic compounds and antibiotics. Newly synthesized LPS is extracted from the inner membrane by the ATP-binding cassette (ABC) transporter $LptB_2FGC$, which places the glycolipid onto a periplasmic protein bridge that connects to the outer membrane. This ABC transporter is structurally unusual in that it associates with an additional protein, LptC. The periplasmic domain of LptC is part of the transporter's bridge while its transmembrane α-helix intercalates into the LPS-binding cavity of the core $LptB_2FG$ transporter. LptC's transmembrane helix affects the in vitro ATPase activity of $LptB_2FG$, but its role in LPS transport in cells remains undefined. Here, we describe two roles of LptC's transmembrane helix in *Escherichia coli*. We demonstrate that it is required to maintain proper levels of LptC and participates in coupling the activity of the ATPase LptB to that of its transmembrane partners LptF/LptG prior to loading LPS onto the periplasmic bridge. Our data support a model in which the association of LptC's transmembrane helix with LptFG creates a nonessential step that slows down the LPS transporter.

KEYWORDS
ABC transporter, glycolipid, lipid transport, membrane biogenesis, transenvelope

1 | INTRODUCTION

The cell envelope of *Escherichia coli* has four major structural components: the inner membrane (IM) surrounding the cytoplasm; the outer membrane (OM), the aqueous compartment between these two membranes known as the periplasm; and the peptidoglycan cell wall that resides in the periplasm (Figure 1a) (Silhavy et al., 2010). Unlike the IM, which is a phospholipid bilayer, the OM of most Gram-negative bacteria contains phospholipids in the inner leaflet and glycolipids known as lipopolysaccharide (LPS) in the outer leaflet (Kamio & Nikaido, 1976). LPS, which is essential in at least some Gram-negative bacteria including *E. coli*, is an amphipathic molecule with three major structural components: Lipid A, an oligosaccharide core, and the O-antigen polysaccharide (Bertani & Ruiz, 2018; Raetz & Whitfield, 2002; Zhang et al., 2013). Tight packing of LPS molecules at the cell surface together with its hydrophilic components create a permeability barrier against hydrophobic molecules including many antimicrobials (Nikaido, 2003). This inherent resistance provided by LPS contributes to the difficulty in treating and developing new antibiotics for Gram-negative bacterial infections (Zgurskaya & Rybenkov, 2020).

LPS is synthesized in the IM and then transported to the OM by the *l*ipo*p*olysaccharide *t*ransport (Lpt) system, which is comprised of LptA-G in *E. coli* (Figure 1a) (Wilson & Ruiz, 2021). The ATP-binding

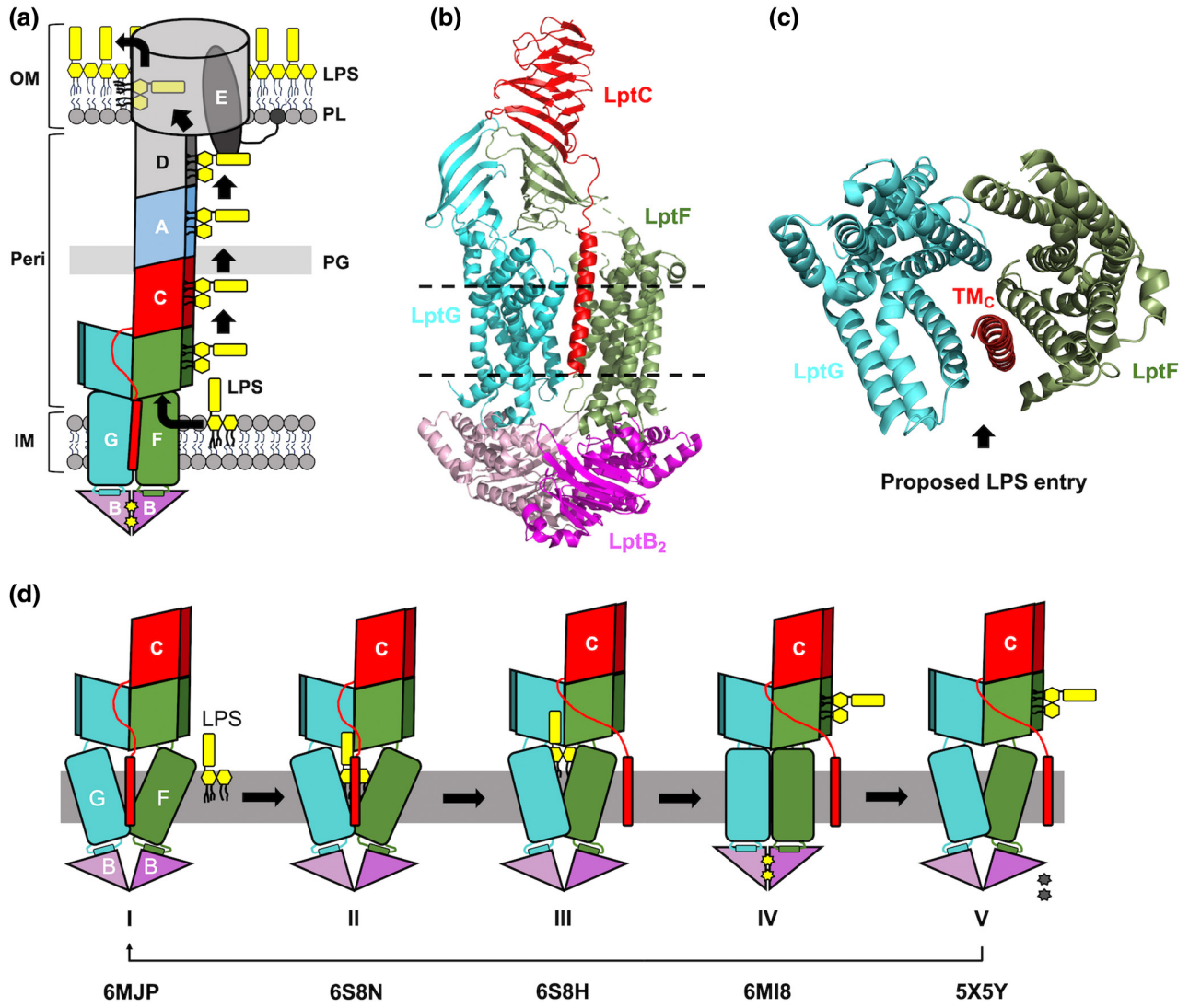

FIGURE 1 Structure and model of the function of the Lpt system. (a) Components of the Lpt system. Binding and hydrolysis of ATP (yellow star bound to LptB) by the ABC transporter $LptB_2FGC$ powers the transport of LPS from the IM, across the periplasm (labeled peri) to the cell surface through the concerted efforts of LptA-G. (b) Crystal structure of $LptB_2FGC$ from *Vibrio cholerae* (PDB ID: 6MJP). Dashed lines represent predicted membrane boundaries. The TM helix is interdigitated between LptF TM5 and LptG TM1. (c) Top-down view from the periplasm of the LPS-binding cavity formed by LptFGC in the structure shown in panel (b) (PDB ID: 6MJP). The periplasmic β-jellyroll domains of LptFGC have been hidden for clarity. The black arrow marks a lateral opening into the cavity. (d) A model depicting LPS extraction from the IM by $LptB_2FGC$. The PDB ID of each $LptB_2FG(C)$ complex is shown below each state (I through V). Notably, structures corresponding to states IV and V lacked LPS; the structure corresponding to state II did not resolve the β-jellyrolls of LptFGC; the structures corresponding to states III and V were solved without LptC, and the structure corresponding to state III did not resolve the β-jellyrolls of LptFG; and the structure corresponding to state IV did not resolve the β-jellyrolls of LptFGC or the location of LptC's TM helix. *I to II*: LPS enters the cavity formed by LptFGC and forms stable contacts with the inner wall. *II to III*: LptC's TM helix is ejected from its position between LptF and LptG, causing a partial cavity collapse and upward movement of LPS. *III to IV*: ATP (yellow stars) binds and $LptB_2$ closes, which facilitates complete LptFG cavity collapse and LPS extraction. LPS is loaded onto the transenvelope bridge at LptF's β-jellyroll. *IV to V*: ATP is hydrolyzed and ADP (gray stars) + P_i (not shown) are released from the NBDs. The reopening of $LptB_2$ opens the LptFG cavity and the system is ready for a new round of transport.

cassette (ABC) transporter $LptB_2FGC$ extracts LPS from the outer leaflet of the IM and places the glycolipid onto a periplasmic protein bridge formed by the periplasmic β-jellyroll domains of LptFCAD (Okuda et al., 2012; Ruiz et al., 2008; Simpson et al., 2015; Sperandeo et al., 2007, 2008). This transenvelope bridge guides LPS to the OM while shielding its acyl chains from the surrounding aqueous periplasm (Chng et al., 2010; Freinkman et al., 2012; Owens et al., 2019; Sherman et al., 2018). Subsequent LPS extraction events at the IM are proposed to push LPS molecules already on the bridge toward the OM (Okuda et al., 2012, 2016; Sherman et al., 2018). Finally, the LptDE OM translocon selectively inserts LPS molecules into the outer leaflet of the OM (Dong et al., 2014; Gu et al., 2015; Lundquist & Gumbart, 2020; Malojcic et al., 2014; May et al., 2015; Qiao et al., 2014).

LPS transport by Lpt is powered from the IM by the $LptB_2FGC$ ABC transporter, which utilizes ATP binding and hydrolysis in the cytoplasm to cyclically extract and load LPS molecules onto the transenvelope bridge (Figure 1) (Okuda et al., 2012, 2016; Ruiz et al., 2008; Sherman et al., 2014; Simpson et al., 2015; Sperandeo et al., 2007, 2008). ABC transporters are ubiquitous in nature and broadly share a conserved structure containing two cytoplasmic nucleotide-binding domains (NBDs), which bind and hydrolyze ATP, and two transmembrane domains (TMDs), which catalyze the transport of substrates (Schmitt & Tampé, 2002). Each NBD is physically connected to one TMD, and the NBD dimer binds two ATP molecules at the dimer interface. Each ATP-binding site is formed by half-sites provided by each NBD. Accordingly, the binding of one ATP molecule to each monomer causes the NBDs to dimerize, forming two complete ATP-binding and hydrolysis sites at the dimer interface (Schmitt & Tampé, 2002). In a process known as NBD–TMD coupling, conformational movements in the NBDs that are caused by the binding and hydrolysis of ATP, and the release of ADP and P_i are physically transmitted to the TMDs, providing them with the mechanical energy necessary for substrate movement and resetting to their ground state (Beis, 2015). This coupling process is largely driven by the association of a "coupling helix" on each TMD with a region in the NBD partner that includes the Q-loop motif (Davidson et al., 2008; Dawson et al., 2007; Hollenstein et al., 2007). Conformational rearrangements in the Q-loop motif are thought to be driven by nucleotide binding and hydrolysis and communicated to the TMD's coupling helices.

In $LptB_2FGC$, a cytoplasmic LptB dimer functions as NBDs, while the IM proteins LptFG constitute the two TMDs (Li et al., 2019; Owens et al., 2019; Ruiz et al., 2008; Sperandeo et al., 2007, 2008; Tang et al., 2019). Both LptF and LptG have six transmembrane (TM) α-helices and one periplasmic β-jellyroll domain. The TM helices of LptFG form a V-shaped cavity that binds LPS to mediate extraction (Figure 1b,c) (Dong et al., 2017; Luo et al., 2017). Recent structural studies have made the surprising discovery that the transmembrane α-helix of LptC, which tethers LptC to the IM, interdigitates into this cavity between LptF TM5 and LptG TM1 (Figure 1b,c), a novel architecture for an ABC transporter (Li et al., 2019; Luo et al., 2021; Owens et al., 2019; Tang et al., 2019). According to the model derived from structural and biochemical evidence, an LPS molecule present in the outer leaflet of the IM enters the LptFGC cavity through a lateral gate located, where LptC's TM interacts with LptF TM5 and LptG TM1 in an ATP-independent manner (Figure 1c, and state II in Figure 1d) (Li et al., 2019, Owens et al., 2019, Tang et al., 2019). In the cavity, LPS forms contacts with LptF and LptG, including the stabilization of the negatively charged phosphates on LPS by a ring of positively charged amino acid residues on LptF and LptG (Bertani et al., 2018; Li et al., 2019; Luo et al., 2021; Owens et al., 2019; Tang et al., 2019). ATP binding is thought to eventually induce the concomitant closure of the LptB dimer and the LPS-binding cavity, squeezing LPS out and somehow loading it onto the periplasmic β-jellyroll fold of LptF (state IV in Figure 1d) (Li et al., 2019; Owens et al., 2019; Simpson et al., 2019; Tang et al., 2019). ATP hydrolysis is proposed to induce the reopening of the LptB dimer and LPS-binding cavity, resetting the transporter for a new round of LPS extraction (state V in Figure 1d) (Sherman et al., 2014; Simpson et al., 2019). Structural studies have also revealed $LptB_2FGC$ bound to LPS in two states: in one, LPS forms few contacts with the LptFGC cavity (state II in Figure 1d) and in the other, LptC's TM helix is no longer associated with LptFG, causing the LPS molecule to slightly elevate within the now smaller substrate-binding cavity, which allows LPS to establish more interactions with residues in LptF and LptG (state III in Figure 1d) (Li et al., 2019, Tang et al., 2019). Based on these observations, the current model for LPS extraction proposes that LPS enters first into the large cavity formed by the TM helices of LptFGC, and then the TM helix of LptC is somehow displaced, priming the transporter for the total collapse of the LptFG cavity once the LptB dimer closes bound to ATP.

The role of the TM helix of LptC in LPS transport is unclear. Purified and reconstituted $LptB_2FG$ complexes lacking LptC or containing an LptC variant without its TM helix exhibit elevated levels of ATP hydrolysis over wild-type $LptB_2FGC$ complexes, suggesting that LptC's TM helix may play a role in modulating the ATPase activity of the transporter (Li et al., 2019; Owens et al., 2019; Tang et al., 2019). In addition, LPS can be crosslinked to LptC's TM helix (Owens et al., 2019). However, swapping LptC's native TM helix for either that of a different IM protein, MalF, or the cleavable signal peptide of the periplasmic protein MalE does not alter the growth or OM permeability of *E. coli* (Villa et al., 2013). Thus, there are no LPS-related in vivo phenotypes associated with the loss of LptC's TM helix whether the rest of the protein remains anchored to the IM or is released into the periplasm, calling into question whether LptC's TM helix participates in LPS transport in cells. Here we revisited this question and found that converting LptC's TM helix into a cleavable signal sequence does not confer observable phenotypes in LPS transport in an otherwise wild-type strain, as previously reported; however, it leads to a decrease in protein levels, likely because the TM helix facilitates interactions with its partners $LptB_2FG$. Moreover, the LptC variant with a cleavable sequence can suppress defects caused by specific *lptBFG* mutant alleles. Our data support a model where LptC's TM helix affects NBD–TMD coupling, slowing down the transport cycle prior to the collapse of the LptFG cavity.

2 | RESULTS

2.1 | The LptC transmembrane α-helix is not widely conserved in Gram-negative bacteria

The ability to cleave or replace LptC's TM without an apparent in vivo phenotype is paradoxical, given that its removal affects the ATPase activity of $LptB_2FG$ in vitro, it intercalates into the LptFG cavity at the predicted entrance gate for LPS, and it can be crosslinked to LPS in cells (Li et al., 2019, Owens et al., 2019, Tang et al., 2019). Since these studies have focused on *γ-Proteobacteria*, we wondered whether

the bitopic nature of LptC is even conserved among Gram-negative bacteria. Aligning the protein sequences of predicted LptC orthologs from a set of distantly related phyla of Gram-negative bacteria including *Pseudomonadota* (α-, β-, γ-, δ-, and ε-*Proteobacteria* classes), *Bacteroidetes*, *Cyanobacteria*, *Deferribacterota*, *Campylobacterota*, *Elusimicrobiota*, and *Thermodesulfobacteriota* revealed that there is a low level of sequence conservation, although all sequences have an N-terminal region rich in hydrophobic residues aligning to the TM helix of LptC from *E. coli* (Figure S1). To look at each phylum more broadly, we compared the LptC protein sequence from *E. coli* strain *K-12* to the NCBI nonredundant protein sequence database, filtering for specific protein sequences assigned within each phylum. Each set of protein sequences was then analyzed through SignalP-5.0, which determines the probability that a given sequence contains a signal peptide, and whether the signal peptide is cleaved to yield a mature periplasmic protein or a lipoprotein (Almagro Armenteros et al., 2019). SignalP predicted that, while individual protein sequences within each phylum may have a high probability of having their TM cleaved or be predicted to mature into lipoproteins, ~75%–100% of sequences are not predicted to undergo a cleavage event except in the α-*Proteobacteria* class, with 55% of the protein sequences predicted to be cleaved at the N-terminal region (Table S1). Conversely, within the same phylum, the γ-*Proteobacteria* class has among the lowest percentages of sequences that were predicted to be cleaved (0.49%) (Table S1). In addition, few sequences were predicted to be processed into lipoproteins (Table S1). Thus, the predictions from SignalP indicate that the majority of LptC homologs are unlikely to be cleaved and would instead retain their bitopic nature. However, the significant variations in the sequence of LptC even within the *Pseudomonadota* highlights the existence of LptC variants in nature that are predicted to be periplasmic proteins or membrane-anchored lipoproteins. Since these predictions suggested that having a membrane-anchoring TM helix (i.e., being a bitopic membrane protein) or even being membrane anchored (via a TM helix or lipid modification) might not be conserved features among LptC homologs, we generated and characterized isogenic strains of *E. coli* producing the three LptC variants that our analysis had predicted to exist among Gram-negative bacteria (i.e., membrane anchored, periplasmic, and lipoprotein) to compare the impact that membrane tethering via a TM helix or a lipid anchor has on protein levels and function.

2.2 | The loss of membrane anchoring causes a decrease in LptC levels

We constructed plasmids carrying various *lptC* alleles that encode LptC variants that are either membrane anchored, periplasmic, or lipoprotein (Figure 2). The pCL-His6-LptC plasmid produces full-length LptC with an added N-terminal histidine tag ($LptC^{FL}$, Figure 2a,b). As shown below, this tagged protein is fully functional. To obtain an LptC variant with a cleavable TM helix (i.e., signal sequence), we built pCL-His6-LptC(K27A), which encodes an alanine substitution at lysine 27 (K27A; numbering refers to untagged wild-type protein) that generates a signal peptidase I recognition sequence after LptC's TM helix (Figure 2a). Cleavage after the substituted alanine should yield the periplasmic $LptC^{\Delta TM}$ variant composed of the periplasmic linker and β-jellyroll domain (Figure 2c). This is the simplest sequence change to test the effect of the loss of the TM helix and is different from those previously tested that did not reveal an effect in LPS transport (Villa et al., 2013). We also constructed pCL-His6-Lipo-LptC by introducing four substitutions (A25L/E26A/K27G/D28C) that generate a lipobox motif on the TM helix of LptC (Figure 2a). The resulting

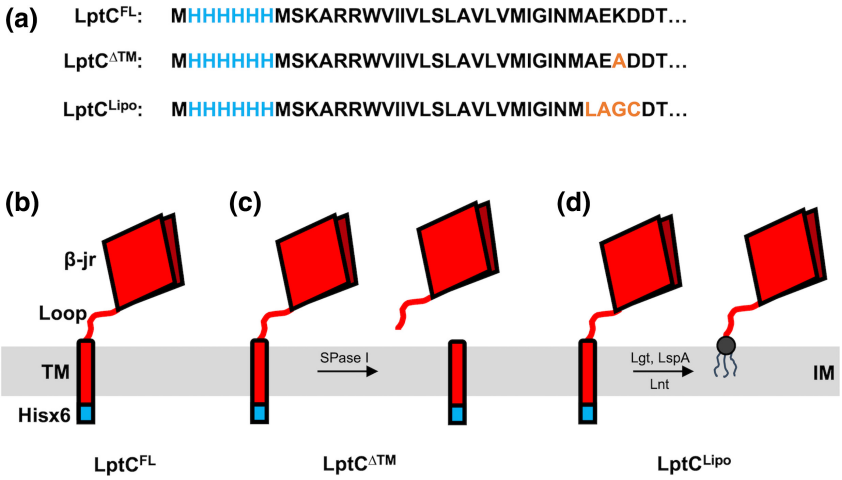

FIGURE 2 Plasmid-encoded LptC variants used in this study. (a) Protein sequences of the first 32 amino acids of wild-type LptC were used to generate the variants shown in panels (b)–(d). The polyhistidine tag is shown in blue. Engineered amino acid substitutions are shown in orange. Panels (b)–(d) show the modifications and processing of the LptC variants encoded in the pCL plasmid. Histidine tags are shown in blue. (b) Full-length LptC ($LptC^{FL}$) is produced from the pCL-His6-LptC plasmid. Domains in LptC are labeled; β-jr refers to β-jellyroll domain and Hisx6 refers to the polyhistidine tag. (c) pCL-His6-LptC(K27A) produces the soluble $LptC^{\Delta TM}$ variant after cleavage of its signal sequence by signal peptidase I (SPase I). (d) The pCL-His6-Lipo-LptC plasmid carries an allele that encodes for a lipobox motif on the signal sequence of *lptC* to produce $LptC^{Lipo}$ after processing by the Lgt, LspA, and Lnt enzymes. The lipidated cysteine at position +1 is shown in dark gray.

variant is predicted to be posttranslationally modified into a lipoprotein (LptC^{Lipo}) such that it should lack the TM helix and instead be anchored to the IM through its tri-acylated cysteine residue at position +1 of the mature lipoprotein (corresponding to C28, Figure 2d) (Grabowicz, 2019). Because the +2 residue in the mature protein is an aspartate (Figure 2a), LptC^{Lipo} should also avoid the Lol system that transports lipoproteins to the OM and thereby stay anchored in the IM (Grabowicz, 2019). As for strains carrying pCL-His6-LptC, we could generate *lptC* haploid strains carrying pCL-His6-LptC(K27A) and pCL-His6-Lipo-LptC by introducing a Δ*lptC* chromosomal allele. Therefore, the three alleles complement the loss of chromosomal *lptC*.

We next analyzed the levels and localization of the plasmid-encoded LptC variants in *lptC* haploid cells. We could barely detect chromosomally encoded LptC in most whole-cell extracts of a control strain by immunoblotting using anti-LptC antiserum but readily detect plasmid-encoded LptC^{FL} and LptC^{Lipo} (Figure 3a). In contrast, we could only detect a weak band corresponding to plasmid-encoded LptC$^{\Delta TM}$, which was predicted to migrate faster if it underwent cleavage of its engineered signal sequence (Villa et al., 2013). Since the antiserum was raised against the periplasmic domain of LptC (Freinkman et al., 2012), our results suggested that the loss of membrane anchoring might lead to degradation of LptC$^{\Delta TM}$, but enough is present to complement the loss of chromosomal *lptC* and it is still present at higher levels than wild-type LptC expressed from the chromosome. We also tested the efficiency of cleavage of LptC^{Lipo} by blotting samples with anti-His-tag antibodies since posttranslational processing into a lipoprotein should cleave off its His_6-TM helix (Figure 2). As expected, we could detect LptC^{FL} in α-His-tag immunoblots (Figure 3b). We could also detect a weaker signal in LptC^{Lipo} samples (Figure 3b). A comparison of the signals obtained for LptC^{FL} and LptC^{Lipo} from

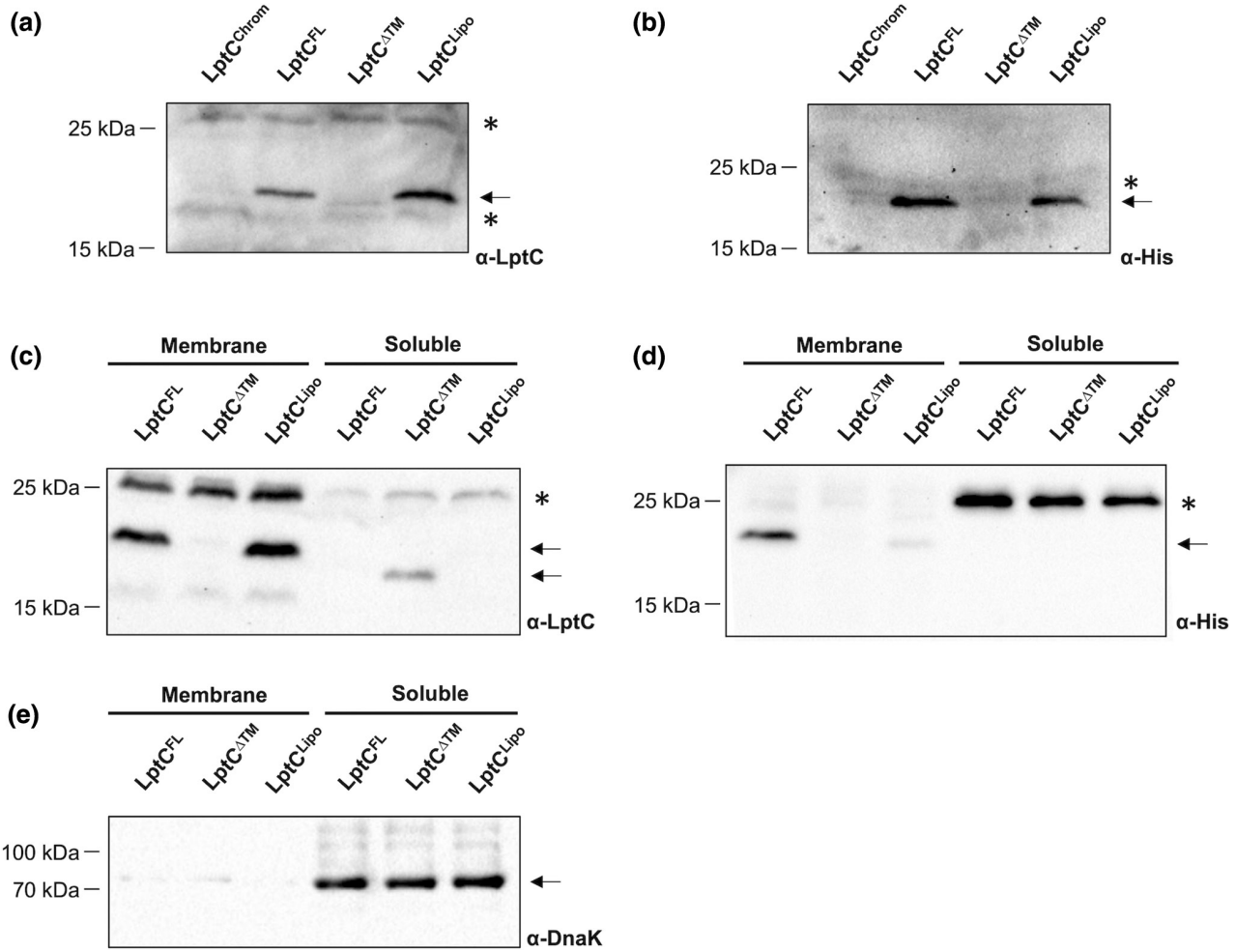

FIGURE 3 Membrane anchoring is required to maintain LptC levels in cells. Protein samples were prepared from haploid mutant strains carrying the chromosomal Δ*lptC* allele and plasmids producing LptC^{FL}, LptC$^{\Delta TM}$, and LptC^{Lipo} and from a wild-type strain (samples labeled LptC^{Chrom}). (a) and (b) Immunoblot of LptC variants using α-LptC (panel a) and α-His-tag (panel b) antibodies. Protein samples were prepared from whole-cell lysates of bacterial cultures in the mid-exponential growth phase. (c) and (d) Immunoblots using the α-LptC antibody (panel c) raised against the soluble portion of LptC or α-His-tag antibody (panel d). Protein samples were collected from bacterial cultures in the mid-exponential growth phase and were separated into membrane and soluble fractions. (e) Immunoblot of the same samples from panels (c) and (d) using antibodies that recognize the cytoplasmic protein DnaK to check for proper cell fractionation. Arrows point to bands corresponding to LptC variants or DnaK. Asterisks indicate nonspecific bands recognized by the antibodies. Markers on the left of each immunoblot show the size of protein standards. LptC protein variant names are indicated above each lane.

LptC and His-tag immunoblots suggested that much of LptC^{Lipo} remains a full-length protein (Figure 3a,b).

Since we predicted that LptC^{FL} and LptC^{Lipo} would be membrane anchored while LptC$^{\Delta TM}$ would be periplasmic, we prepared concentrated samples from the membrane and soluble cellular fractions and analyzed them by immunoblot blotting using α-LptC and α-His-tag antibodies (Figure 3c,d). As expected, using the α-LptC antiserum, we detected LptC^{FL} and LptC^{Lipo} in the membrane fraction but not the soluble fraction, while mature LptC$^{\Delta TM}$ was detectable only in the soluble fraction of LptC$^{\Delta TM}$ cells and we could not detect chromosomally encoded LptC (Figures 3c and S2). In agreement with results obtained with whole-cell extracts (Figure 3a), levels of LptC$^{\Delta TM}$ were decreased compared with LptC^{FL} and LptC^{Lipo} (Figure 3c). In some biological repeats of samples from haploid cells that only encode for LptC$^{\Delta TM}$, we could also detect a very weak band that migrated similarly to LptC^{FL} in the membrane fraction on LptC immunoblots but not on His-tag immunoblots (Figure 3c,d), which likely corresponds to pro-LptC$^{\Delta TM}$ that is yet to be processed. In contrast, we could always detect, as in whole-cell samples, a signal in the membrane fraction of cells producing LptC^{Lipo} on His-tag immunoblots (Figure 3d). The abundance of this species that still contains its TM helix is significant (10%–15% of that detected from LptC^{FL} samples in α-His-tag immunoblots) (Figure 3d), again suggesting that not all the LptC^{Lipo} is modified into a lipoprotein. This finding calls into question the ability of pCL-His6-Lipo-LptC to complement the loss of chromosomal *lptC* since at least 10% of the protein is not modified as a lipoprotein. Indeed, we will report in a separate study evidence supporting that the modified LptC^{Lipo} variant is nonfunctional and will not use LptC^{Lipo} in the rest of the present study. Despite this caveat, our data show that levels of LptC are decreased when the protein is not anchored to the membrane; furthermore, this anchoring does not have to be exclusively mediated by its native TM helix as revealed by the results obtained with LptC^{Lipo}. The remainder of this work will focus on the characterization of haploid strains producing LptC$^{\Delta TM}$.

2.3 | The *lptC*$^{\Delta TM}$ allele does not confer defects in growth or LPS transport on its own

We next monitored the growth of haploid strains harboring the plasmid-encoded *his$_6$-lptC* and *his$_6$-lptC*(*K27A*) (herein *his$_6$-lptC*$^{\Delta TM}$) alleles and assessed their level of resistance to antibiotics whose entry across the OM is limited by LPS using disc diffusion assays. Defects in LPS transport can negatively affect growth and resistance depending on severity (Lundstedt, Kahne, et al., 2021). The *his$_6$-lptC*$^{\Delta TM}$ haploid strain and that carrying pCL-His6-LptC (producing LptC^{FL}) grew similarly in LB (Figure 4a). Both strains also showed comparable resistance to hydrophobic antibiotics (Figure 4b), corroborating earlier findings that plasmid-encoded periplasmic LptC is fully functional (Villa et al., 2013).

Given that our immunoblot analyses showed that levels of LptC decrease upon loss of membrane anchoring (Figure 3), we wondered if the failure to detect mutant phenotypes caused by *his$_6$-lptC*$^{\Delta TM}$ resulted from the higher than native production of LptC$^{\Delta TM}$ resulting from the plasmid. To address this possibility, we introduced the *lptC*(*K27A*) mutation into native chromosomal *lptC* using CRISPR. The resulting chromosomal *lptC*$^{\Delta TM}$ strain behaves like its wild-type parent and the haploid strain carrying plasmid-encoded *his$_6$-lptC*$^{\Delta TM}$ with respect to growth and OM permeability (Figure 4c,d). As with wild-type LptC produced from the chromosome, we could not detect this periplasmic variant when produced from the chromosome using immunoblotting (data not shown). In subsequent studies, we used the mutant strain carrying chromosomally encoded *lptC*$^{\Delta TM}$ unless otherwise noted.

2.4 | A targeted approach to investigate the role of LptC's TM in LPS transport

Several structural and biochemical studies have shown that LptC's TM helix: (i) intercalates between TM helix 1 of LptG and TM helix 5 of LptF, (ii) can be crosslinked to LPS in vivo, and (iii) has a negative effect on the ATPase activity of purified LptB$_2$FGC complexes (Li et al., 2019; Owens et al., 2019; Tang et al., 2019). In vivo studies have not identified a functional role of LptC's TM helix in LPS transport, but these functional studies cannot distinguish between two possibilities: (i) that the LptC's TM helix has no role in the function of LptB$_2$FGC in cells or (ii) that the LptC's TM helix plays a nonessential role in LPS transport that is not detectable by simply removing LptC TM's helix in an otherwise wild-type cell. According to the current model for LPS transport by LptB$_2$FGC (Figure 1d), removing LptC's TM helix would alter the resting state (state I, Figure 1d) and possibly LPS entry into the substrate-binding cavity, and eliminate the state where LPS only makes few initial contacts with the cavity (state II, Figure 1d), but not later downstream steps. We reasoned that we could interrogate the proposed role of LptC's TM helix in cells by combining *lptC*$^{\Delta TM}$ with other *lpt* alleles that affect specific steps of the extraction cycle. We expected to uncover synthetic phenotypes (synergy or suppression) between two mutations if they were functionally linked in any of the steps of the transport cycle.

2.5 | The *lptC*$^{\Delta TM}$ allele does not affect interactions between LptG and LPS

In the current model for LPS transport by LptB$_2$FGC, the LptC's TM helix must be removed from the LptFG cavity for the complex to transition from a lower LPS-binding state to one with higher LPS-binding affinity (states II and III, respectively, Figure 5a). Based on this model, *lptC*$^{\Delta TM}$ would eliminate the lower LPS-binding affinity state. We therefore speculated that *lptC*$^{\Delta TM}$ might have an effect on mutants defective in LPS-LptG contacts, possibly helping them by eliminating the lower LPS-binding affinity state. Residues K34, K40, and K41 in LptG are part of a larger network of amino acids that bind to LPS (Bertani et al., 2018; Li et al., 2019). Replacing these residues with aspartates decreases LPS transport presumably by destabilizing LPS binding within the LptFG cavity due to

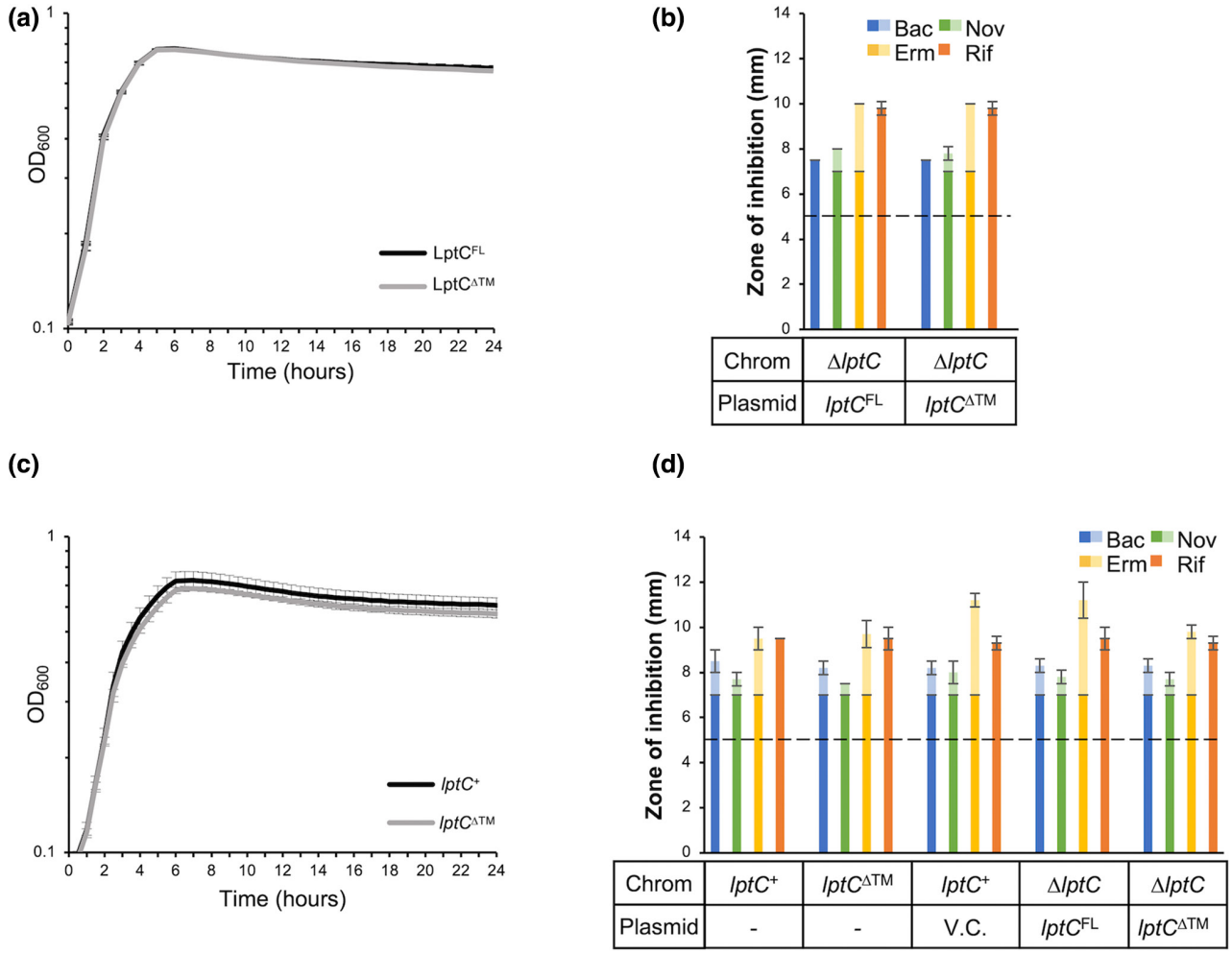

FIGURE 4 Loss of membrane anchoring of LptC does not change growth or OM permeability to hydrophobic antibiotics. (a) Growth curve of haploid strains of *E. coli* carrying the chromosomal Δ*lptC* allele and plasmid-encoded his_6-*lptC* ($LptC^{FL}$) or his_6-$lptC^{\Delta TM}$ ($LptC^{\Delta TM}$) in LB at 37°C. (b) OM permeability of strains from panel (a) was assessed using disc diffusion assays. Values represent the diameter of the zone of inhibition of growth (darker color on the graph) or of partial inhibition of growth (lighter color on the graph) surrounding the antibiotic disc. The dashed line indicates the diameter (7 mm) of the antibiotic disc. Chrom refers to chromosomal, Bac to bacitracin, Nov to novobiocin, Erm to erythromycin, and Rif to rifampicin. (c) Growth curve of *E. coli* strains carrying either the chromosomal $lptC^{+}$ allele or the chromosomal $lptC^{\Delta TM}$ allele in LB at 37°C. (d) OM permeability of strains from panels (a) and (c) and vector control (V.C.) was assessed by disc diffusion assay. Data are presented as the average and standard deviation (error bars) of three independent experiments.

the clashing charges between the aspartates on LptG and the phosphates on the Lipid A moiety of LPS (Bertani et al., 2018). Notably, the *lptG*(*K34D*) allele confers stronger defects than either *lptG*(*K40D*) or *lptG*(*K41D*), and structural studies showed contacts between LptG's residue K34 and LPS in states II and III (Figure 5a), whereas K40 and K41 contact LPS only during state III (after LptC's TM helix has been removed from the cavity) (Bertani et al., 2018, Li et al., 2019). We found that the $lptC^{\Delta TM}$ *lptG*(*K34D*) double mutant was more sensitive to several hydrophobic antibiotics than *lptG*(*K34D*) single mutant (Figure 5b and Table S2). However, we attribute this synthetic defect to the decreased protein levels caused by $lptC^{\Delta TM}$ since we do not observe the same increase in antibiotic susceptibility when *lptG*(*K34D*) is introduced into a strain carrying plasmid-borne $lptC^{\Delta TM}$, which produced higher levels of $LptC^{\Delta TM}$ (Figure 3 and Table S2). Furthermore, when we combined $lptC^{\Delta TM}$ with *lptG*(*K40D*) and *lptG*(*K41D*), $lptC^{\Delta TM}$ did not change the sensitivity caused by these *lptG* alleles (Figure 5c, Table S2). Taken together, our results suggest that LPS entry into the LptFG cavity and the subsequent stabilization of LPS–cavity interactions mediated by LptG/K34, LptG/K40, and LptG/K41 are unaffected by the presence or absence of LptC's TM helix (Figure 5a).

2.6 | The $lptC^{\Delta TM}$ allele suppresses specific mutations in lptB, lptF, and lptG that affect NBD-TMD coupling

In the current model, the closure of the LPS-binding cavity in $LptB_2FGC$ complexes is a two-step process. First, the larger LptFGC-LPS cavity becomes smaller after the removal of LptC's TM helix

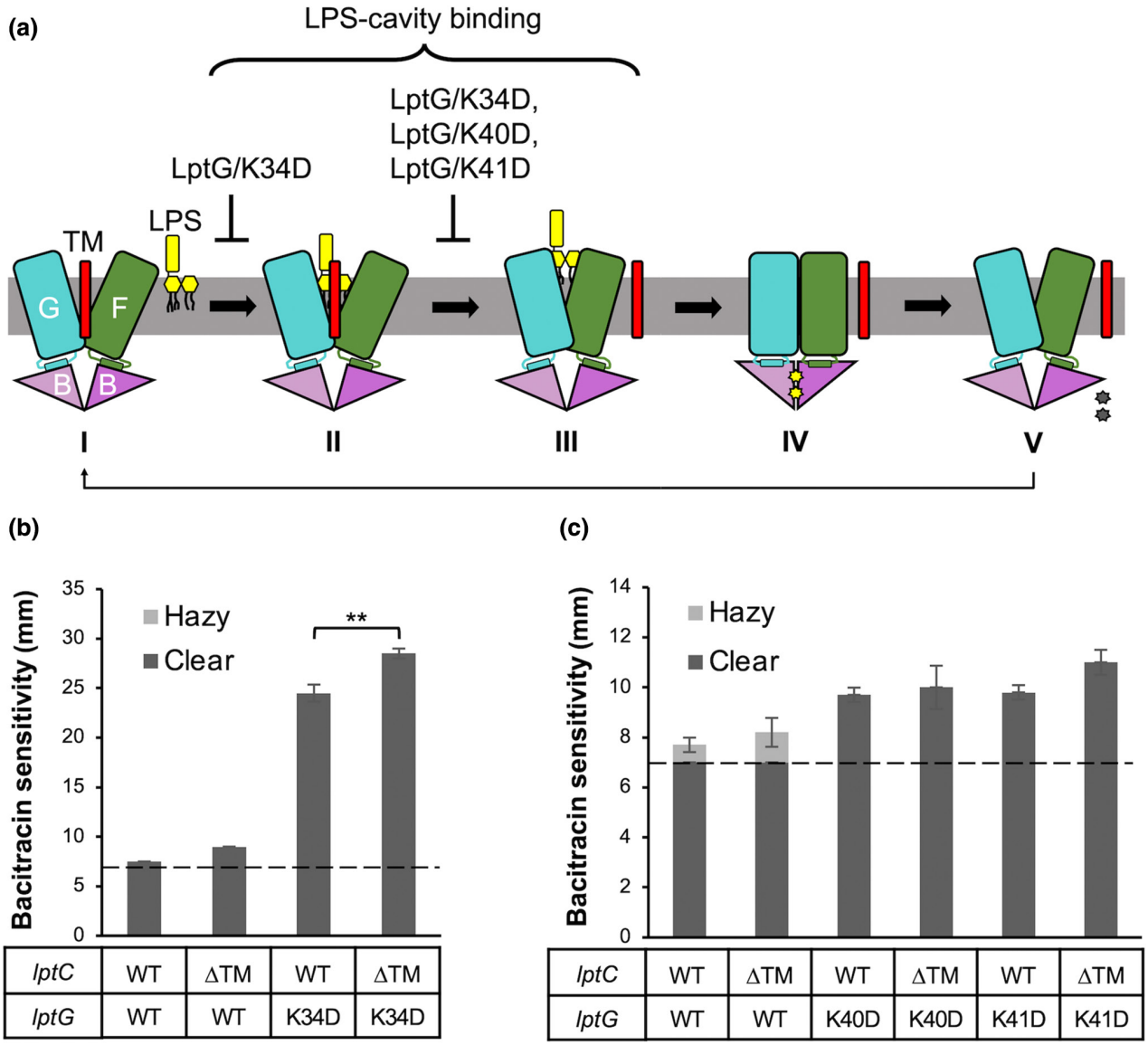

FIGURE 5 Effect of the loss of LptC's TM helix in *lptG* mutants defective in interactions with LPS. (a) Model for LPS extraction by $LptB_2FGC$. The β-jellyroll domains have been hidden for simplicity. Steps, where interactions between LPS and the substrate-binding cavity occur, are marked above the model, in addition to mutant *lpt* alleles affecting these steps. (b) and (c) Disc diffusion assays to probe OM permeability of mutant strains defective in interactions between LPS and residues in LptG present in the substrate-binding during states II and III (panel b) or only state III (panel c). Mutants carry either chromosomal wild-type *lptC* (WT) or $lptC^{\Delta TM}$ (ΔTM) alleles and plasmid-borne *lptG*(*K34D*) (panel b) or either *lptG*(*K40D*) or *lptG*(*K41D*) (panel c) alleles. Clear zones indicate no growth surrounding the antibiotic disc; hazy zones indicate partial clearing surrounding the antibiotic disc. The dashed line indicates the diameter (7 mm) of the antibiotic disc. Data represent the average and standard deviation of three independent experiments. Differences of sensitivity that were less than 2 mm were not analyzed for statistical significance since we consider them insignificant as they fall within or near the range of measuring error. $^{**}p < .01$.

through an unknown mechanism (transition between states II and III, Figure 6a); then, the LptFG-LPS cavity collapses, extruding and placing LPS on the Lpt bridge (state IV, Figure 6a). According to this model, $lptC^{\Delta TM}$ might exhibit genetic interactions with alleles affecting the transition of the transporter between states II and III, but not those affecting downstream steps (Figure 6a). Previously, our laboratory identified several substitutions in LptBFG that we proposed to affect the closure and reopening of the LPS-binding cavity in the $LptB_2FGC$ transporter (Lundstedt et al., 2020; Lundstedt, Simpson, et al., 2021; Simpson et al., 2019). We therefore combined them with the $lptC^{\Delta TM}$ allele to further interrogate the proposed role of LptC's TM helix in LPS transport.

As stated earlier, the Q-loop motif in the NBDs (i.e., ATPase LptB) and the coupling helices in the TMDs (i.e., LptFG) are thought to function in NBD–TMD coupling in ABC transporters (Figure 6b) (Davidson et al., 2008; Luo et al., 2017; Simpson et al., 2016). Accordingly, residue E86 in the Q-loop of LptB, and residues E84 and E88 in the coupling helices of LptF and LptG, respectively, had been identified as important in coupling the closure of the LptB dimer with that of the LPS-binding cavity in LptFG (Lundstedt et al., 2020; Lundstedt, Simpson,

et al., 2021; Simpson et al., 2016). However, it is not clear whether these residues affect the partial cavity closure caused by the removal of LptC's TM helix (transition from state II to III, Figure 6a) and/or the total closure of the cavity (transition from state III to IV, Figure 6a). We combined *lptC*$^{\Delta TM}$ with the total loss-function *lptB*(*E86A*) allele, and the partial loss-of-function *lptB*(*E86Q*), *lptF*(*E84A*), and *lptG*(*E88A*) alleles. We found that while *lptC*$^{\Delta TM}$ cannot suppress the lethality conferred by *lptB*(*E86A*), it fully suppresses the OM permeability defects caused by *lptB*(*E86Q*) (Figure 6c). The *lptC*$^{\Delta TM}$ allele also partially suppresses the sensitivity to antibiotics individually caused by *lptF*(*E84A*) and *lptG*(*E88A*) (Figure 6d). Moreover, while growth of an *lptF*(*E84A*) *lptG*(*E88A*) double mutant strain is restricted to a minimal medium because faster growth in a rich medium imposes too great a demand for the defective $LptB_2FGC$ complex, this conditional lethality is suppressed by *lptC*$^{\Delta TM}$. The resulting *lptC*$^{\Delta TM}$ *lptF*(*E84A*) *lptG*(*E88A*) triple mutant can grow in LB medium but still exhibits sensitivity to antibiotics that is indicative of severe defects in LPS transport (Figure 6d). These results provide the first evidence supporting that LptC's TM helix affects LPS transport in *E. coli* cells. We do not think that this suppression can be explained by the decrease in LptC–LptF/G interactions that may result from the loss of the TM helix since these interactions are required for transport (Freinkman et al., 2012; Sherman et al., 2018). Furthermore, the fact that suppression is allele-specific suggests that LptC's TM helix affects specific steps in the cycle. Furthermore, if the current transport model is correct (Figure 6a), our data suggest that the fully suppressed *lptB*(*E86Q*) allele only affects the transition between states II and III, while the partially suppressed *lptF*(*E84A*) and *lptG*(*E88A*) [and possibly the unsuppressed *lptB*(*E86A*) allele] affect this and one or more additional steps.

The last step of the LPS extraction cycle involves the hydrolysis of ATP to reopen the $LptB_2$ dimer and LptFG cavity (state V, Figure 6a). Specific alterations to the C-terminal loop of LptB at the dimer interface cause defects in the reopening of the LptB dimer and, consequently, the LptFG cavity (Figure 6b) (Simpson et al., 2019). One example is the extension of the C-terminal loop with a polyhistidine epitope encoded by the *lptB-his*$_8$ allele. Notably, cosuppression of LPS transport defects has been observed between alleles that alter this C-terminal loop and those changing specific residues in the signature helix of LptB [e.g., *lptB*(*R144H*)] as well as those in a network of residues physically linking the distant signature helix and the C-terminal loop of LptB (Figure 6b) (Simpson et al., 2019). In NBDs of ABC transporters, the signature helix immediately follows the signature motif, which is part of the ATP-binding site in the closed LptB dimer (Davidson et al., 2008; Schmitt & Tampé, 2002). It was proposed that the cosuppressing changes affect the opening and closing of the LptB dimer in opposite ways: *lptB-his*$_8$ mutants favor the closed dimer state (facilitating the transition between states III and IV while disfavoring that between states IV and V, Figure 6a), whereas *lptB*(*R144H*) disfavors the closed dimer state (disfavoring the transition between states III and IV while favoring that between states IV and V, Figure 6a) (Simpson et al., 2019). We reasoned that if LptC's TM helix functions prior to the closing and reopening of the LptB dimer, as proposed in the current model (Figure 6a), *lptC*$^{\Delta TM}$ would not affect *lptB*(*R144H*) and *lptB-his*$_8$ mutants. Indeed, *lptC*$^{\Delta TM}$ did not change either the inability of the *lptB*(*R144H*) mutant to grow in an LB medium or the OM permeability defects conferred by *lptB-his*$_8$ (Figure 6e). Together with our data support that LptC's TM helix participates in LPS transport in *E. coli* as suggested by the model shown in Figure 6a.

2.7 | The *lptC*$^{\Delta TM}$ allele suppresses defects in ATP binding by LptB

Structural and in vivo data support that closure of the LptB dimer (after binding ATP and prior ATP hydrolysis) triggers the concomitant closure of the LPS-binding cavity in the $LptB_2FGC$ complex, causing the transfer of LPS to the Lpt bridge (state IV, Figure 6a); then, ATP hydrolysis occurs, leading to the coordinated reopening of the LptB dimer and LptFG cavity (state V, Figure 6a) so that the transport cycle can restart (Li et al., 2019; Owens et al., 2019; Simpson et al., 2019; Tang et al., 2019). As in other ABC transporters, two ATP molecules bind each LptB dimer, and each of the two ATP-binding sites is composed of half-sites provided by each LptB monomer. One half-site is mainly composed of the A-loop and Walker A domains of one monomer, whereas the other is mainly composed of the signature motif of the other monomer (Figure 6b). ATP binding should precede closure of the LptB dimer, likely first occurring at the half-site containing the A-loop and Walker A domains in each monomer (Ambudkar et al., 2006; Davidson et al., 2008; Smith et al., 2002). Structural studies have not revealed at what state(s) in the transport cycle ATP molecules bind to LptB in the open dimer conformation, but we know that ATP binding and hydrolysis can occur in vitro in purified $LptB_2FGC$ complexes even in the absence of LPS (Li et al., 2019). Moreover, purified $LptB_2FG$ and $LptB_2FGC^{\Delta TM}$ complexes show higher ATPase activity than wild-type $LptB_2FGC$ complexes (Li et al., 2019, Owens et al., 2019, Tang et al., 2019). Given that our data so far show that *lptC*$^{\Delta TM}$ affects mutants that are defective in the transition between states II and III but not those affecting steps downstream in the pathway, we reasoned that *lptC*$^{\Delta TM}$ might help us determine if ATP can bind prior to state III (Figure 6a). We made an alanine substitution in LptB's residue Y13, a conserved residue in the A-loop of NBDs of ABC transporters that contributes to ATP binding by interacting with the adenine ring of ATP through its aromatic side chain (Figure 6b) (Ambudkar et al., 2006; Tang et al., 2019). We found that a haploid strain expressing *lptB*(*Y13A*) from a plasmid exhibits increased sensitivity to antibiotics that are mostly suppressed by *lptC*$^{\Delta TM}$ (Figure 7, Table S2). Based on epistasis analysis, we propose that, in order to see this suppressive effect, ATP must be able to bind $LptB_2FGC$ prior to the removal of the LptC's TM helix from the LPS-binding cavity. If ATP could only bind after LptC's TM helix is already removed, the LptC$^{\Delta TM}$ should not suppress the defects conferred by *lptB*(*Y13A*).

3 | DISCUSSION

The $LptB_2FGC$ is functionally and structurally different from most ABC transporters. ABC transporters typically translocate or flip

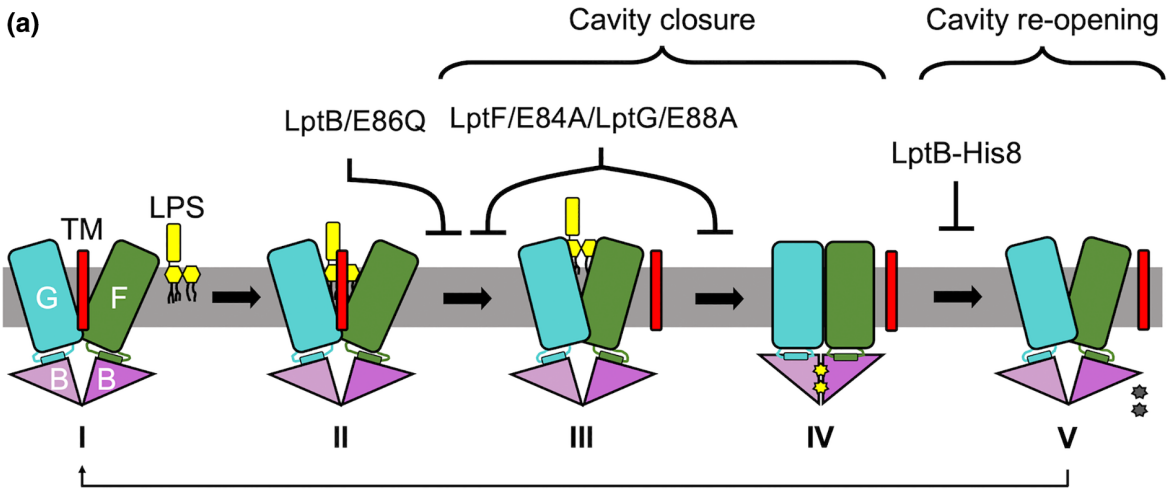

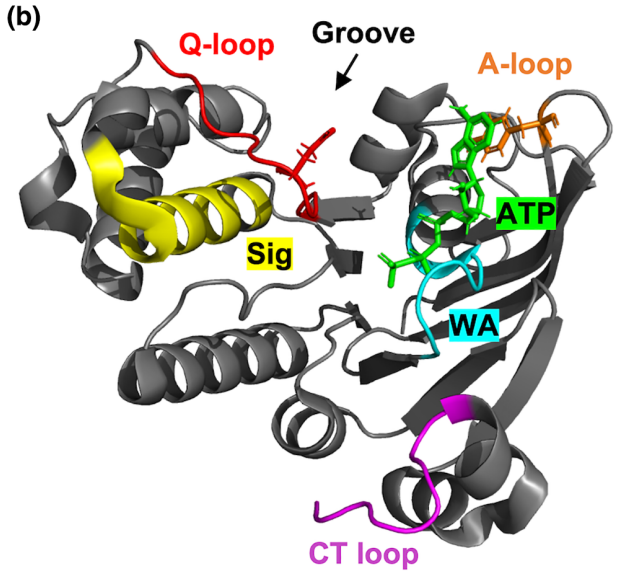

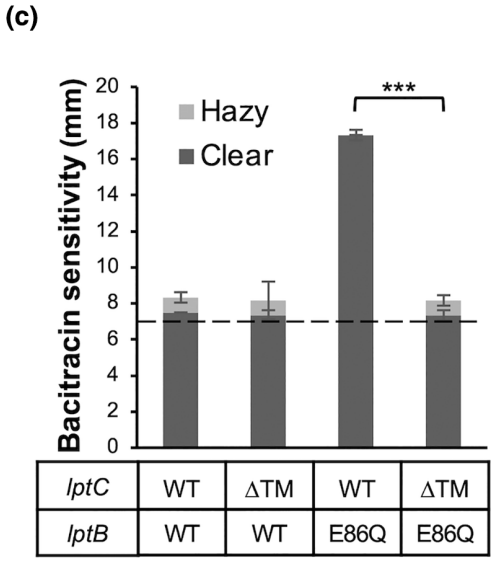

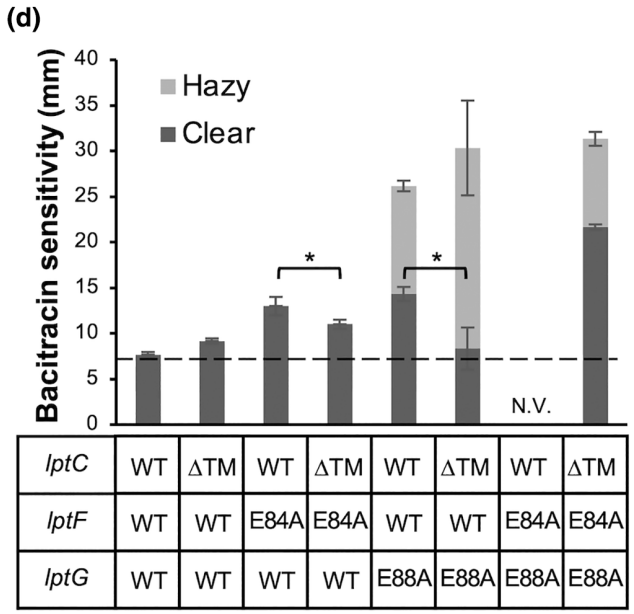

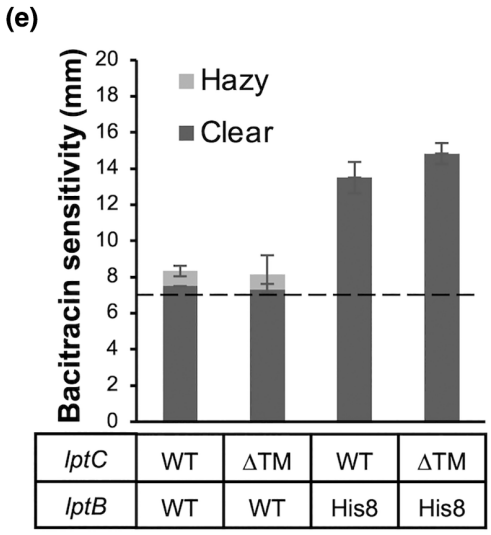

substrates across membranes and their substrates diffuse away into aqueous or membrane environments after translocation (Dawson et al., 2007). In contrast, $LptB_2FGC$ extracts a glycolipid from a membrane and places it onto a protein bridge where it is thought to push a stream of previously extracted substrates toward their destination, the OM (Wilson & Ruiz, 2021). Structurally, $LptB_2FGC$

FIGURE 6 The LptC$^{\Delta TM}$ variant strongly suppresses NBD–TMD coupling defects, but not defects in cavity closure or opening. (a) Model for LPS extraction by LptB$_2$FGC. The β-jellyroll domains have been hidden for simplicity. The cavity closure and cavity reopening steps are marked above the model, in addition to mutant *lpt* alleles affecting these steps. (b) Crystal structure of catalytically inactive His$_8$-LptB(E163Q) from *E. coli* in complex with ATP (PDB ID: 6MBN). Relevant regions of the NBD are colored and labeled. Sig = signature motif and helix. WA = Walker A. CT loop = C-terminal region loop. The side chains of residues E86 in the Q-loop and Y13 of the A-loop are shown. (c–e) OM permeability was assessed by disc diffusion assays in mutants carrying chromosomal wild-type *lptC* (WT) or *lptC*$^{\Delta TM}$ (ΔTM) alleles and plasmid-borne *lptB*(*E86Q*) (panel c), *lptF*(*E84A*) and *lptG*(*E88A*) (panel d), and *lptB-his*$_8$ (panel e). Clear zones and hazy zones indicate no growth or partial clearing surrounding the antibiotic disc, respectively. The dashed line indicates the diameter (7 mm) of the antibiotic disc. Data represent the average and standard deviation of three independent experiments. Differences of sensitivity that were less than 2 mm were not analyzed for statistical significance since we consider them insignificant as they fall within or near the range of measuring error. $^{*}p < .05$. $^{***}p < .001$. N.V., not viable.

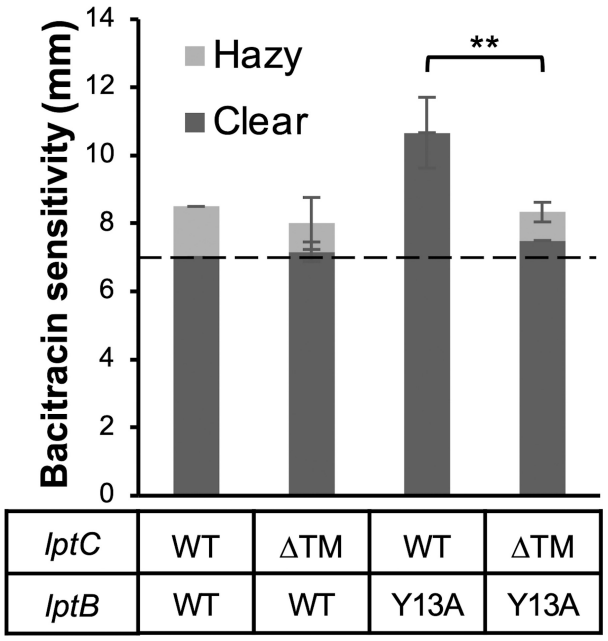

FIGURE 7 The *lptC*$^{\Delta TM}$ allele suppresses defects in ATP binding. OM permeability of mutants carrying the wild-type, *lptB*(*Y13A*), and *lptC*$^{\Delta TM}$ alleles was determined using disc diffusion assays. The *lptC*$^{\Delta TM}$ allele suppresses the defects conferred by *lptB*(*Y13A*). Clear zones indicate no growth surrounding the antibiotic disc; hazy zones indicate partial clearing surrounding the antibiotic disc. The dashed line indicates the diameter (7 mm) of the antibiotic disc. Data represent the average and standard deviation of three independent experiments. Differences of sensitivity that were less than 2 mm were not analyzed for statistical significance since we consider them insignificant as they fall within or near the range of measuring error. $^{**}p < .01$.

is unusual in two main ways. First, the periplasmic domains of both LptF and LptC are part of the Lpt protein bridge linking the IM and OM (Freinkman et al., 2012; Sherman et al., 2018). Second, the substrate-binding cavity in LptB$_2$FGC is not only formed by its TMDs but also contains the TM helix of the bitopic protein LptC (Li et al., 2019; Owens et al., 2019; Tang et al., 2019). Intriguingly, while evidence from in vitro ATPase assays, structural studies, and in vivo LPS crosslinking experiments have called for a functional role for LptC's TM helix and shaped our current model for LPS extraction by LptB$_2$FGC, the removal of this TM helix has no apparent effect on LPS transport in otherwise wild-type *E. coli* cells (Li et al., 2019; Owens et al., 2019; Tang et al., 2019; Villa et al., 2013). Here, we have presented evidence supporting that LptC's TM helix has two physiological roles in *E. coli*: to maintain LptC protein levels likely by facilitating its association with LptB$_2$FG and to participate in NBD–TMD coupling by creating an early step in the LPS extraction cycle that slows down LptB$_2$FGC.

Our data show that cellular levels of LptC significantly decrease when its TM helix is removed by signal peptidase, which releases the soluble portion of LptC into the periplasm. Furthermore, maintenance of LptC levels does not require its specific native TM helix. Tethering of the periplasmic domain to the IM by other means suffices, as supported by the fact that levels of LptC^{Lipo} do not decrease even when most of this variant lacks a TM helix and instead is anchored to the membrane via a lipid moiety. Likely, being able to diffuse through the periplasm after processing makes the LptC$^{\Delta TM}$ variant susceptible to degradation because its association with LptB$_2$FG is less efficient than when it is anchored to the IM, where LptFG resides. There are two previous observations that support this proposal. Copurification experiments from *E. coli* cells by Villa et al. showed that LptB$_2$FG copurified less efficiently with a periplasmic LptC variant (in which the native TM helix had been replaced with the signal sequence of the periplasmic protein MalE [or MBP]) compared with a variant anchored to the IM via a TM helix of the IM protein MalF (Villa et al., 2013). In addition, *lpt* mutations that affect the formation of periplasmic Lpt bridges lead to the degradation of periplasmic LptA by an unknown protease(s) (Martorana et al., 2021; Moura et al., 2020; Sperandeo et al., 2008, 2011), given that LptA is structurally similar to the periplasmic β-jellyroll of LptC, it is possible that periplasmic LptC$^{\Delta TM}$ has the same fate when is not interacting with the β-jellyroll of LptF. Accordingly, we propose that a cellular function of LptC's TM helix is to anchor LptC in the IM so that it can efficiently form complexes with LptB$_2$FG.

Despite the decrease in LptC levels that removing its TM causes, *E. coli* cells producing such periplasmic LptC variants do not exhibit defects in LPS transport to the cell surface, thus questioning whether the previously reported association of LptC's TM helix with LPS and the TM helices of LptFG are functionally relevant in cells (Villa et al., 2013). Recognizing the limitations of the current methods to monitor LPS transport in cells, we undertook a genetic strategy that we thought could reveal even subtle changes in LPS transport that would be inappreciable in an otherwise wild-type strain: to remove the LptC's TM helix in cells producing mutant LptB$_2$FG complexes that are defective in different steps in the extraction cycle; we

expected that if LptC's TM helix affected one or more steps in LPS extraction, its removal could lead to suppression or negative synergistic effects in mutants affecting the same step(s). Indeed, we found genetic interactions between *lptC*$^{\Delta TM}$ and specific alleles affecting ATP binding by LptB and NBD-TMD coupling. Thus, LptC's TM participates in LPS transport in cells. Notably, our data are not limited to providing support for the prevailing model for LPS extraction from the IM but also refine it by proposing that (i) ATP binding to LptB can occur when the LptC's TM helix is associated with LptFG and (ii) the coupling helices of LptFG and residue E86 in LptB participate in the removal of LptC's TM helix from the LPS-binding cavity.

So far, the only structures of $LptB_2FG(C)$ complexes in which nucleotide molecules bound to LptB have been resolved are those in which nonhydrolyzable ATP analogs have trapped the complex in the postextraction state IV (Figure 8) (Li et al., 2019; Tang et al., 2019). The fact that *lptC*$^{\Delta TM}$ suppresses *lptB*(*Y13A*), which causes a defect in the A-loop that binds the adenine group of ATP, indicates that ATP binding can occur when LptC's TM helix is participating in the transport cycle and thus can occur at states I and/or II (Figure 8) (Ambudkar et al., 2006). We do not mean to imply that ATP can only bind when LptC's TM helix is present in the LptFG cavity; clearly, it can occur when it is not since the *lptC*$^{\Delta TM}$ single mutant does not exhibit LPS transport defects.

Our data have also shown a functional link between LptC's TM helix and NBD–TMD coupling since *lptC*$^{\Delta TM}$ suppresses *lptB*(*E86Q*) and *lptF*(*E84A*)/*lptG*(*E88A*). We previously had concluded that these *lptB/F/G* mutants are defective in the closure of the LPS-binding cavity (Lundstedt et al., 2020; Lundstedt, Simpson, et al., 2021; Simpson et al., 2016). Combining our previous and present data, we propose that, in wild-type complexes, the removal of LptC's TM helix involves NBD–TMD coupling and specifically residue E86 in LptB and the coupling helices of LptFG. Thus, LPS entry into the cavity alone is not sufficient to properly displace LptC's TM helix. Furthermore, that *lptB*(*E86Q*) is completely suppressed by *lptC*$^{\Delta TM}$, while the more defective *lptB*(*E86A*) allele is not, and that *lptC*$^{\Delta TM}$ can only partially suppress *lptF*(*E84A*)/*lptG*(*E88A*) suggest that residue E86 of LptB and residues E84 and E88 in the coupling helices of LptF and LptG, respectively, play additional roles in LPS transport. Indeed, earlier work implicated these residues in the transition to state IV that occurs when the LptB dimer closes around two ATP molecules to trigger the total collapse of the LPS-binding cavity and movement of LPS to the Lpt bridge (Lundstedt et al., 2020; Lundstedt, Simpson, et al., 2021; Simpson et al., 2016).

Why would the LPS extraction cycle include a step that appears to be unnecessary? Biochemical studies have shown that the removal of LptC's TM helix leads to an increase in ATP hydrolysis by $LptB_2FGC$ complexes (Li et al., 2019; Owens et al., 2019; Tang et al., 2019). Thus, the unnecessary step created by the insertion of LptC's helix in the LPS-binding cavity slows down the transport cycle. Our data have revealed genetic interactions between LptC's TM helix and ATP binding to LptB in the open-dimer conformation, the Q-loop of LptB, and the coupling helices of LptFG. We therefore suggest that the intercalation of LptC's TM helix into the substrate-binding cavity allows LptB (through its residue E86) to properly coordinate the total collapse of the cavity and release of LPS into the periplasmic bridge. Since LptB's activity has been previously shown to be influenced by residues in the TM helices of LptFG and the periplasmic region of LptF (Baeta et al., 2021; Benedet et al., 2016; Lundstedt et al., 2020), and the physical structure of the Lipid A and core regions of LPS (Lundstedt, Simpson, et al., 2021), it remains unknown whether LptC's TM helix prevents premature closing of the substrate-binding cavity to ensure proper binding of LPS and ATP and/or coordination with the placement of LPS onto the β-jellyroll of LptF. Moreover, if the Lpt system functions akin to a PEZ candy dispenser and LPS travels as a stream, this slow step might be necessary to maintain a certain flow rate along the Lpt bridge. It is also possible that once an Lpt bridge is formed and transport is triggered, the reintercalation of LptC's TM helix with the helices of LptF and LptG (transition between states V and I) is not obligatory at each cycle and is adaptable to maintain LPS flow or does not occur during active transport until the system is turned off.

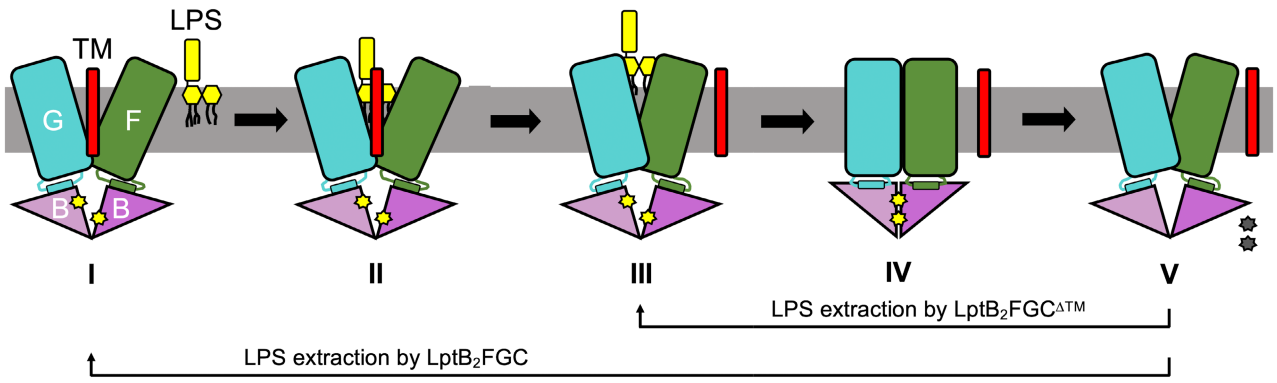

FIGURE 8 Revised model for LPS extraction from the IM by $LptB_2FGC$. Our data support the involvement of LptC's TM in LPS transport by $LptB_2FGC$ in cells. We also propose that ATP can bind to LptB when LptC's TM is intercalated in the LptFG cavity (states I and II). In $LptB_2FGC^{\Delta TM}$ complexes, the transport cycle is shortened as shown by the arrow. Whether wild-type complexes can transition from states V to III as $LptB_2FGC^{\Delta TM}$ complexes remain undetermined. See Discussion for details.

4 | EXPERIMENTAL PROCEDURES

4.1 | Growth conditions

Unless otherwise noted, strains were grown at 37°C in lysogeny broth (LB) or M63 minimal medium, which was supplemented with 0.2% (wt/vol) glucose. Cells were grown on liquid cultures with aeration or on solid media on 1.5% agar plates. When appropriate, growth media were supplemented with spectinomycin (LB: 100 μg/ml, M63: 200–400 μg/ml), ampicillin (125 μg/ml), tetracycline (25 μg/ml), kanamycin (30 μg/ml), isopropyl β-D-1-thiogalactopyranoside (IPTG, 0.16 mM), or 5-bromo-4-chloro-3-indolyl β-D-galactopyranoside (X-Gal, 33 μg/ml).

4.2 | Strain and plasmid construction

Table S3 shows the strains used in this study. P1*vir* transduction was used to introduce chromosomally encoded alleles. The Δ*lptB*::*frt* and Δ*lptFG*::*frt* alleles were cotransduced with previously described *tet2* and *yjgN*::*tet* alleles, respectively, by selecting for tetracycline and screening for the loss of wild-type *lptB* or *lptFG* by PCR. When necessary, the kanamycin cassette disrupting *lpt* genes was removed using the temperature-sensitive pCP20 plasmid, which encodes Flp recombinase (Cherepanov & Wackernagel, 1995). The chromosomal *lptC*(*K27A*) allele was generated through the scarless Cas9-assisted recombineering system (no-SCAR) (Reisch & Prather, 2015, 2017). The resulting allele was then introduced into a wild-type strain by P1*vir* transduction and confirmed by DNA sequencing.

To construct pCL-His6-LptC, his_6-*lptC* was introduced into pCL-His6-LptB, kindly provided by the Kahne laboratory, to replace his_6-*lptB* (Freinkman et al., 2012; Simpson et al., 2016). The pCL-His6-LptB plasmid (Simpson et al., 2016) was digested with AvrII and XbaI restriction enzymes and dephosphorylated with Antarctic phosphatase (all enzymes were purchased from New England Biolabs). The his_6-*lptC* allele was obtained by digesting pET23/42-His6-LptC (Freinkman et al., 2012) with AvrII and XbaI and ligated into the cut pCL expression vector with T4 DNA ligase to generate pCL-His6-LptC. Sanger sequencing was used to confirm proper plasmid construction. Plasmids encoding LptC variants, pCL-His6-LptC(K27A) and pCL-His6-Lipo-LptC, were constructed via site-directed mutagenesis using Phusion high-fidelity DNA polymerase (New England Biolabs), pCL-His6-LptC as a template, and primers listed in Table S4. Mutations were similarly introduced into *lptB* and *lptFG* using pET23/42LptB and pBAD18LptFG3 as a template (Bertani et al., 2018; Lundstedt et al., 2020; Sherman et al., 2014; Simpson et al., 2016). Mutagenized plasmids were introduced into electrocompetent DH5α cells and confirmed by Sanger DNA sequencing. Relevant strains were transformed with plasmids using chemical transformation (Chung et al., 1989).

4.3 | Complementation analysis

The ability of plasmid-encoded *lptC* alleles to complement an *lptC* chromosomal deletion was tested by introducing Δ*lptC*::*kan* (Chng et al., 2010) by P1*vir* transduction and selection for transductants on plates containing kanamycin and spectinomycin. Transductants were verified by PCR. Complementation studies on *lptB* and *lptFG* alleles were conducted as previously described using blue-white screening of characterization strains carrying pRC7CatSacBLptC or pRC7KanLptFG plasmids, respectively (Sherman et al., 2014; Simpson et al., 2016). Haploid strains carrying alleles that complemented were identified as white colonies and used for phenotypic characterization.

4.4 | Growth curves

Strains were first grown overnight in 5 ml of LB to similar densities, as determined by optical density at 600 nm (OD_{600}), and diluted 1:1000 in LB. A 100-μl sample of each dilution was transferred to a 96-well microtiter plate (Fisher) that was incubated for 24 h at 37°C with double-orbital shaking at 807 RPM. Growth was monitored by taking OD_{600} measurements every 30 or 60 min. Data are representative of at least three biological replicates.

4.5 | Antibiotic-sensitivity assays

Bacterial strains were grown overnight in 5 ml of either LB or M63 (supplemented with 0.2% glucose) supplemented where necessary with the appropriate antibiotics. For saturated cultures, 50 μl of LB or 100 μl of M63 cultures were transferred to a sterile glass tube. If there was a noticeable difference in cell density, the inoculum volume was normalized by OD_{600} using $V_{sample} = \frac{OD_{WT} \times (50\ \mu l)}{OD_{sample}}$ for cultures grown in LB, or $V_{sample} = \frac{OD_{WT} \times (100\ \mu l)}{OD_{sample}}$ for cultures grown in M63. Each sample was mixed with 4 ml of molten LB top agar (0.75% agar) and poured over an LB agar plate. Discs containing antibiotics were placed on top of the LB top agar, and plates were incubated overnight at 37°C. The diameter of the zone of inhibition of growth around each disc was recorded in millimeters. The OM permeability of each strain was assayed against bacitracin (10 U), novobiocin (30 μg), erythromycin (15 μg), and rifampicin (5 μg) discs (BD BBL Sensi-Disc). Data are representative of at least three independent bacterial cultures.

4.6 | Analysis of protein levels and localization

Protein samples were prepared from whole-cell lysates of bacterial cultures grown in exponential phase and normalized by cell density as previously described (Sherman et al., 2014). Alternatively, protein

samples were separated into membrane and soluble fractions as follows. Strains grown overnight in 5 ml of LB were diluted 1:50 into 50 ml of LB and grown to exponential phase. At an OD_{600} of 0.6–0.8, cells were pelleted at 3220 rcf for 10 min at 4°C. Cell pellets (kept on ice for the rest of the preparation) were resuspended in 2 ml Tris (pH 7.4), 1 mM EDTA, 0.5X protease inhibitor cocktail (Sigma), and lysed by passage through a One-Shot pressure cell (Constant Systems) two times at 30,000 PSI. Cell debris was removed from the resulting lysate via centrifugation at 2000 rcf for 10 min at 4°C. A 1 ml sample of the supernatant was transferred to an ultracentrifuge tube and centrifuged at 100,000 rpm for 1 h at 4°C in a TLA 120.2 rotor (Beckman Coulter). The pellet, containing the membrane fraction, was resuspended in 75 µl of membrane solubilization buffer (300 mM NaCl, 20 mM Tris pH 7.4, 10% glycerol, 5 mM $MgCl_2$) supplemented with 7.5 µl of 10% DDM. This resuspension was centrifuged at 3220 rcf for 10 min at 4°C to eliminate any residual debris or unsolubilized proteins and the supernatant was mixed with 75 µl of the protein-loading buffer (67.5 mM Tris pH 6.8, 6.75% SDS, 5% 2-mercaptoethanol, 2% glycerol, 0.05% bromophenol blue). This concentrated mixture was diluted as necessary in the protein-loading buffer to be of equal volume soluble cellular fraction samples prior to electrophoresis. The supernatant from ultracentrifugation, containing the soluble cellular fraction, was frozen overnight. After thawing, it was concentrated at 60°C using the V-AQ setting on a speed vacuum (Eppendorf). The resulting pellet was resuspended in 250 µl of the protein-loading buffer. Samples from whole-cell extracts and cellular fractionations were boiled for 10 min and proteins were separated by electrophoresis on 12% SDS polyacrylamide gels and transferred to polyvinylidene difluoride (PVDF) membranes (Roche Diagnostics, Basel, Switzerland). PVDF membranes were probed with rabbit anti-LptC (1:10,000 dilution) (Freinkman et al., 2012), mouse anti-His (1:1000 dilution; Sigma), or mouse anti-DnaK (1:10,000 dilution; Lifespan Biosciences) primary antibodies at 4°C with gentle agitation overnight and with anti-rabbit (1:10,000 dilution; GE Amersham) or anti-mouse (1:10,000 dilution; GE Healthcare Life Sciences) horseradish peroxidase-conjugated secondary antibodies, respectively, for 1 h at room temperature. Signal was developed using Clarity Western ECL substrate (Bio-Rad) and immunoblots were imaged using the ChemiDoc CRS+system. The ImageLab 5.2.1 software (Bio-Rad) was used in subsequent image analysis to quantify band intensity where applicable.

4.7 | Bioinformatic analyses of LptC orthologs

The protein sequence for wild-type LptC from *E. coli* strain *K-12* was analyzed through NCBI BLAST (Altschul et al., 1990) using the default parameters except for the modifications outlined below. In order to find protein sequences of LptC homologs within a specific phylum, wild-type LptC was filtered against the phylum in question by adding in each phylum (or class, where applicable) individually under the options for "Choose Search Set" on the NCBI BLAST suite. Under "Algorithm Parameters," the number of maximum target sequences was increased to 5000. Every sequence returned by the BLAST search was collected onto a text file and inserted into SignalP-5.0, which can analyze multiple sequences at once (Almagro Armenteros et al., 2019). The results were compiled in Table S1.

AUTHORS' CONTRIBUTION

Conceptualization of study: Andrew Wilson and Natividad Ruiz; *Data acquisition*: Andrew Wilson; *Data analysis*: Andrew Wilson and Natividad Ruiz; *Writing of the manuscript*: Andrew Wilson and Natividad Ruiz.

ACKNOWLEDGMENTS

The authors thank Daniel Kahne for providing the α-LptC antibody, Rebecca M. Davis for preparing media, as well as former and current members of the Ruiz laboratory for the discourse surrounding this study. This work was supported by the National Institute of General Medical Sciences awards T32-GM086252 (to A. W.) and R01-GM100951 (to N. R.). Open access funding enabled and organized by ProjektDEAL.

ETHICS STATEMENT

The work presented here did not include human or animal subjects nor human or animal data. Thus, no formal consent or approval was necessary.

CONFLICT OF INTEREST

The authors do not have a conflict of interest to declare.

DATA AVAILABILITY STATEMENT

The data that supports the findings of this study are available in the supplementary material of this article.

ORCID

Natividad Ruiz https://orcid.org/0000-0002-6369-2206

REFERENCES

Almagro Armenteros, J.J., Tsirigos, K.D., Sonderby, C.K., Petersen, T.N., Winther, O., Brunak, S. et al. (2019) SignalP 5.0 improves signal peptide predictions using deep neural networks. *Nature Biotechnology*, *37*, 420–423.

Altschul, S.F., Gish, W., Miller, W., Myers, E.W. & Lipman, D.J. (1990) Basic local alignment search tool. *Journal of Molecular Biology*, *215*, 403–410.

Ambudkar, S.V., Kim, I.W., Xia, D. & Sauna, Z.E. (2006) The A-loop, a novel conserved aromatic acid subdomain upstream of the Walker a motif in ABC transporters, is critical for ATP binding. *FEBS Letters*, *580*, 1049–1055.

Baeta, T., Giandoreggio-Barranco, K., Ayala, I., Moura, E., Sperandeo, P., Polissi, A. et al. (2021) The lipopolysaccharide-transporter complex LptB2FG also displays adenylate kinase activity in vitro dependent on the binding partners LptC/LptA. *The Journal of Biological Chemistry*, *297*, 101313.

Beis, K. (2015) Structural basis for the mechanism of ABC transporters. *Biochemical Society Transactions*, *43*, 889–893.

Benedet, M., Falchi, F.A., Puccio, S., Di Benedetto, C., Peano, C., Polissi, A. et al. (2016) The lack of the essential LptC protein in the trans-envelope lipopolysaccharide transport machine is circumvented by

suppressor mutations in LptF, an inner membrane component of the *Escherichia coli* transporter. *PLoS One*, *11*, e0161354.

Bertani, B. & Ruiz, N. (2018) Function and biogenesis of lipopolysaccharides. *EcoSal Plus*, *8*, ESP-0001-2018.

Bertani, B.R., Taylor, R.J., Nagy, E., Kahne, D. & Ruiz, N. (2018) A cluster of residues in the lipopolysaccharide exporter that selects substrate variants for transport to the outer membrane. *Molecular Microbiology*, *109*, 541–554.

Cherepanov, P.P. & Wackernagel, W. (1995) Gene disruption in *Escherichia coli*: TcR and KmR cassettes with the option of Flp-catalyzed excision of the antibiotic-resistance determinant. *Gene*, *158*, 9–14.

Chng, S.S., Gronenberg, L.S. & Kahne, D. (2010) Proteins required for lipopolysaccharide assembly in *Escherichia coli* form a transenvelope complex. *Biochemistry*, *49*, 4565–4567.

Chung, C.T., Niemela, S.L. & Miller, R.H. (1989) One-step preparation of competent *Escherichia coli*: transformation and storage of bacterial cells in the same solution. *Proceedings of the National Academy of Sciences of the United States of America*, *86*, 2172–2175.

Davidson, A.L., Dassa, E., Orelle, C. & Chen, J. (2008) Structure, function, and evolution of bacterial ATP-binding cassette systems. *Microbiology and Molecular Biology Reviews*, *72*, 317–364.

Dawson, R.J., Hollenstein, K. & Locher, K.P. (2007) Uptake or extrusion: crystal structures of full ABC transporters suggest a common mechanism. *Molecular Microbiology*, *65*, 250–257.

Dong, H., Tang, X., Zhang, Z. & Dong, C. (2017) Structural insight into lipopolysaccharide transport from the gram-negative bacterial inner membrane to the outer membrane. *Biochimica et Biophysica Acta - Molecular and Cell Biology of Lipids*, *1862*, 1461–1467.

Dong, H., Xiang, Q., Gu, Y., Wang, Z., Paterson, N.G., Stansfeld, P.J. et al. (2014) Structural basis for outer membrane lipopolysaccharide insertion. *Nature*, *511*, 52–56.

Freinkman, E., Okuda, S., Ruiz, N. & Kahne, D. (2012) Regulated assembly of the transenvelope protein complex required for lipopolysaccharide export. *Biochemistry*, *51*, 4800–4806.

Grabowicz, M. (2019) Lipoproteins and their trafficking to the outer membrane. *EcoSal Plus*, *8*, ESP-0038-2018.

Gu, Y., Stansfeld, P.J., Zeng, Y., Dong, H., Wang, W. & Dong, C. (2015) Lipopolysaccharide is inserted into the outer membrane through an intramembrane hole, a lumen gate, and the lateral opening of LptD. *Structure*, *23*, 496–504.

Hollenstein, K., Dawson, R.J. & Locher, K.P. (2007) Structure and mechanism of ABC transporter proteins. *Current Opinion in Structural Biology*, *17*, 412–418.

Kamio, Y. & Nikaido, H. (1976) Outer membrane of *Salmonella typhimurium*: accessibility of phospholipid head groups to phospholipase C and cyanogen bromide activated dextran in the external medium. *Biochemistry*, *15*, 2561–2570.

Li, Y., Orlando, B.J. & Liao, M. (2019) Structural basis of lipopolysaccharide extraction by the LptB2FGC complex. *Nature*, *567*, 486–490.

Lundquist, K.P. & Gumbart, J.C. (2020) Presence of substrate aids lateral gate separation in LptD. *Biochimica et Biophysica Acta - Biomembranes*, *1862*, 183025.

Lundstedt, E., Kahne, D. & Ruiz, N. (2021) Assembly and maintenance of lipids at the bacterial outer membrane. *Chemical Reviews*, *121*, 5098–5123.

Lundstedt, E.A., Simpson, B.W. & Ruiz, N. (2020) LptB-LptF coupling mediates the closure of the substrate-binding cavity in the LptB2 FGC transporter through a rigid-body mechanism to extract LPS. *Molecular Microbiology*, *114*, 200–213.

Lundstedt, E.A., Simpson, B.W. & Ruiz, N. (2021) Lipopolysaccharide transport involves long-range coupling between cytoplasmic and periplasmic domains of the LptB2FGC extractor. *Journal of Bacteriology*, *203*, e00618-00620.

Luo, Q., Shi, H. & Xu, X. (2021) Cryo-EM structures of LptB2FG and LptB2FGC from *Klebsiella pneumoniae* in complex with lipopolysaccharide. *Biochemical and Biophysical Research Communications*, *571*, 20–25.

Luo, Q., Yang, X., Yu, S., Shi, H., Wang, K., Xiao, L. et al. (2017) Structural basis for lipopolysaccharide extraction by ABC transporter LptB2FG. *Nature Structural & Molecular Biology*, *24*, 469–474.

Malojcic, G., Andres, D., Grabowicz, M., George, A.H., Ruiz, N., Silhavy, T.J. et al. (2014) LptE binds to and alters the physical state of LPS to catalyze its assembly at the cell surface. *Proceedings of the National Academy of Sciences of the United States of America*, *111*, 9467–9472.

Martorana, A.M., Moura, E., Sperandeo, P., Di Vincenzo, F., Liang, X., Toone, E. et al. (2021) Degradation of components of the Lpt transenvelope machinery reveals LPS-dependent Lpt complex stability in *Escherichia coli*. *Frontiers in Molecular Biosciences*, *8*, 758228.

May, J.M., Sherman, D.J., Simpson, B.W., Ruiz, N. & Kahne, D. (2015) Lipopolysaccharide transport to the cell surface: periplasmic transport and assembly into the outer membrane. *Philosophical Transactions of the Royal Society of London. Series B, Biological Sciences*, *370*, 20150027.

Moura, E., Baeta, T., Romanelli, A., Laguri, C., Martorana, A.M., Erba, E. et al. (2020) Thanatin impairs lipopolysaccharide transport complex assembly by targeting LptC-LptA interaction and decreasing LptA stability. *Frontiers in Microbiology*, *11*, 909.

Nikaido, H. (2003) Molecular basis of bacterial outer membrane permeability revisited. *Microbiology and Molecular Biology Reviews*, *67*, 593–656.

Okuda, S., Freinkman, E. & Kahne, D. (2012) Cytoplasmic ATP hydrolysis powers transport of lipopolysaccharide across the periplasm in *E. coli*. *Science*, *338*, 1214–1217.

Okuda, S., Sherman, D.J., Silhavy, T.J., Ruiz, N. & Kahne, D. (2016) Lipopolysaccharide transport and assembly at the outer membrane: the PEZ model. *Nature Reviews Microbiology*, *14*, 337–345.

Owens, T.W., Taylor, R.J., Pahil, K.S., Bertani, B.R., Ruiz, N., Kruse, A.C. et al. (2019) Structural basis of unidirectional export of lipopolysaccharide to the cell surface. *Nature*, *567*, 550–553.

Qiao, S., Luo, Q., Zhao, Y., Zhang, X.C. & Huang, Y. (2014) Structural basis for lipopolysaccharide insertion in the bacterial outer membrane. *Nature*, *511*, 108–111.

Raetz, C.R. & Whitfield, C. (2002) Lipopolysaccharide endotoxins. *Annual Review of Biochemistry*, *71*, 635–700.

Reisch, C.R. & Prather, K.L. (2015) The no-SCAR (Scarless Cas9 assisted recombineering) system for genome editing in *Escherichia coli*. *Scientific Reports*, *5*, 15096.

Reisch, C.R. & Prather, K.L.J. (2017) Scarless Cas9 assisted recombineering (no-SCAR) in *Escherichia coli*, an easy-to-use system for genome editing. *Current Protocols in Molecular Biology*, *117*, 31 38 31–31 38 20.

Ruiz, N., Gronenberg, L.S., Kahne, D. & Silhavy, T.J. (2008) Identification of two inner-membrane proteins required for the transport of lipopolysaccharide to the outer membrane of *Escherichia coli*. *Proceedings of the National Academy of Sciences of the United States of America*, *105*, 5537–5542.

Schmitt, L. & Tampé, R. (2002) Structure and mechanism of ABC transporters. *Current Opinion in Structural Biology*, *12*, 754–760.

Sherman, D.J., Lazarus, M.B., Murphy, L., Liu, C., Walker, S., Ruiz, N. et al. (2014) Decoupling catalytic activity from biological function of the ATPase that powers lipopolysaccharide transport. *Proceedings of the National Academy of Sciences of the United States of America*, *111*, 4982–4987.

Sherman, D.J., Xie, R., Taylor, R.J., George, A.H., Okuda, S., Foster, P.J. et al. (2018) Lipopolysaccharide is transported to the cell surface by a membrane-to- membrane protein bridge. *Science*, *359*, 798–801.

Silhavy, T.J., Kahne, D. & Walker, S. (2010) The bacterial cell envelope. *Cold Spring Harbor Perspectives in Biology*, *2*, a000414.

Simpson, B.W., May, J.M., Sherman, D.J., Kahne, D. & Ruiz, N. (2015) Lipopolysaccharide transport to the cell surface: biosynthesis and extraction from the inner membrane. *Philosophical Transactions*

of the Royal Society of London. Series B, Biological Sciences, *370*, 20150029.

Simpson, B.W., Owens, T.W., Orabella, M.J., Davis, R.M., May, J.M., Trauger, S.A. et al. (2016) Identification of residues in the lipopolysaccharide ABC transporter that coordinate ATPase activity with extractor function. *mBio*, *7*, e01729-16.

Simpson, B.W., Pahil, K.S., Owens, T.W., Lundstedt, E.A., Davis, R.M., Kahne, D. et al. (2019) Combining mutations that inhibit two distinct steps of the ATP hydrolysis cycle restores wild-type function in the lipopolysaccharide transporter and shows that ATP binding triggers transport. *mBio*, *10*, e01931-19.

Smith, P.C., Karpowich, N., Millen, L., Moody, J.E., Rosen, J., Thomas, P.J. et al. (2002) ATP binding to the motor domain from an ABC transporter drives formation of a nucleotide Sandwich dimer. *Molecular Cell*, *10*, 139–149.

Sperandeo, P., Cescutti, R., Villa, R., Di Benedetto, C., Candia, D., Deho, G. et al. (2007) Characterization of lptA and lptB, two essential genes implicated in lipopolysaccharide transport to the outer membrane of *Escherichia coli*. *Journal of Bacteriology*, *189*, 244–253.

Sperandeo, P., Lau, F.K., Carpentieri, A., De Castro, C., Molinaro, A., Deho, G. et al. (2008) Functional analysis of the protein machinery required for transport of lipopolysaccharide to the outer membrane of *Escherichia coli*. *Journal of Bacteriology*, *190*, 4460–4469.

Sperandeo, P., Villa, R., Martorana, A.M., Samalikova, M., Grandori, R., Deho, G. et al. (2011) New insights into the Lpt machinery for lipopolysaccharide transport to the cell surface: LptA-LptC interaction and LptA stability as sensors of a properly assembled transenvelope complex. *Journal of Bacteriology*, *193*, 1042–1053.

Tang, X., Chang, S., Luo, Q., Zhang, Z., Qiao, W., Xu, C. et al. (2019) Cryo-EM structures of lipopolysaccharide transporter LptB2FGC in lipopolysaccharide or AMP-PNP-bound states reveal its transport mechanism. *Nature Communications*, *10*, 4175.

Villa, R., Martorana, A.M., Okuda, S., Gourlay, L.J., Nardini, M., Sperandeo, P. et al. (2013) The *Escherichia coli* Lpt transenvelope protein complex for lipopolysaccharide export is assembled via conserved structurally homologous domains. *Journal of Bacteriology*, *195*, 1100–1108.

Wilson, A. & Ruiz, N. (2021) Transport of lipopolysaccharides and phospholipids to the outer membrane. *Current Opinion in Microbiology*, *60*, 51–57.

Zgurskaya, H.I. & Rybenkov, V.V. (2020) Permeability barriers of gram-negative pathogens. *Annals of the New York Academy of Sciences*, *1459*, 5–18.

Zhang, G., Meredith, T.C. & Kahne, D. (2013) On the essentiality of lipopolysaccharide to gram-negative bacteria. *Current Opinion in Microbiology*, *16*, 779–785.

SUPPORTING INFORMATION

Additional supporting information can be found online in the Supporting Information section at the end of this article.

How to cite this article: Wilson, A. & Ruiz, N. (2022). The transmembrane α-helix of LptC participates in LPS extraction by the $LptB_2FGC$ transporter. *Molecular Microbiology*, *118*, 61–76. https://doi.org/10.1111/mmi.14952